The Astrophysical Journal, 802:120 (10pp), 2015 April 1 doi:10.1088/0004-637X/802/2/120

GRAVITATIONAL MICROLENSING BY NEUTRON STARS AND RADIO PULSARS: EVENT RATES, TIMESCALE DISTRIBUTIONS, AND MASS MEASUREMENTS

S. Dai[1,2], M. C. Smith[3], M. X. Lin[1], Y. L. Yue[4], G. Hobbs[2], and R. X. Xu[1,5]
[1] School of Physics and State Key Laboratory of Nuclear Physics and Technology, Peking University, Beijing 100871, China; daishi@pku.edu.cn
[2] CSIRO Astronomy and Space Science, Australia Telescope National Facility, Box 76 Epping NSW 1710, Australia
[3] Shanghai Astronomical Observatory, Chinese Academy of Sciences, Shanghai 200030, China; msmith@shao.ac.cn
[4] National Astronomical Observatories, Chinese Academy of Sciences, Beijing 100012, China
[5] Kavli Institute for Astronomy and Astrophysics, Peking University, Beijing 100871, China
Received 2014 December 4; accepted 2015 February 8; published 2015 April 1

ABSTRACT

We investigate properties of Galactic microlensing events in which a stellar object is lensed by a neutron star. For an all-sky photometric microlensing survey, we determine the number of lensing events caused by $\sim 10^5$ potentially observable radio pulsars to be ~ 0.2 yr^{-1} for 10^{10} background stellar sources. We expect a few detectable events per year for the same number of background sources from an astrometric microlensing survey. We show that such a study could lead to precise measurements of radio pulsar masses. For instance, if a pulsar distance could be constrained through radio observations, then its mass would be determined with a precision of $\sim 10\%$. We also investigate the timescale distributions for neutron star events, finding that they are much shorter than had been previously thought. For photometric events toward the Galactic center that last ~ 15 days, around 7% will have a neutron star lens. This fraction drops rapidly for longer timescales. Away from the bulge region we find that neutron stars will contribute $\sim 40\%$ of the events that last less than ~ 10 days. These results are in contrast to earlier work which found that the maximum fraction of neutron star events would occur on timescales of hundreds of days.

Key words: gravitational lensing: micro – pulsars: general – stars: neutron

1. INTRODUCTION

Neutron stars (NSs), as the densest observable objects in the universe, allow us to study diverse phenomena in astrophysics and also probe fundamental physics at extremely high density. For instance, determining whether pulsar-like compact objects are NSs or quark stars would have profound implications on the physics of condensed matter and on the nature of the strong interaction (e.g., Weber 2005; Xu 2010, for a review).

Determining NS masses is essential for constraining properties of their inner structure. The existence of high-mass NSs places strong constraints on the equation of state, while extremely low-mass NSs help distinguish self-bound quark stars from gravity-bound NSs. Recent precise high-mass measurements of PSRs J0348+0432 and J1614-2230 significantly constrained the equation of state of NSs and improved our understanding of pulsar-like compact objects (Demorest et al. 2010; Özel et al. 2010; Lai & Xu 2011; Antoniadis et al. 2013). However, up to now, all precise mass measurements are from observations of binary pulsars. Determining masses for isolated NSs is challenging, but knowing the mass distribution for such NSs is important as it may be different from binary NSs.

Gravitational microlensing has been suggested as a way to measure the masses of isolated NSs (e.g., Horvath 1996; Schwarz & Seidel 2002; Dai et al. 2010). There are two kinds of microlensing phenomena that occur when the line of sight to a distant object passes close to an intervening massive object. The first is known as photometric microlensing, which is observed as the temporal brightening of the background star. For photometric microlensing events, the photometric magnification, A, depends on the angular separation between the lens and the source in units of the angular Einstein radius, $u = \theta_{\rm sl}/\theta_{\rm E}$, as $A \sim 1 + 2/u^4$ (Mao & Paczynski 1996). A typical angular Einstein radius for a stellar microlensing event in the Galaxy is approximately 1 mas. The second is known as astrometric microlensing and is observed as the angular shift, S, of the apparent position of the background star. For angular separations larger than the angular Einstein radius, $\theta_{\rm E}$, the shift $S \sim \theta_{\rm E}/u$ (e.g., Belokurov & Evans 2002, hereafter BE02). Therefore, the cross-section for astrometric events will be much larger than for photometric events because the detectability of astrometric events is not as strongly dependent on u. However, it is currently impractical to carry out large area astrometric microlensing surveys.

The Optical Gravitational Lensing Experiment (OGLE; Udalski 2003) is an ongoing photometric microlensing survey. The third phase of this project, OGLE-III, monitored about 3×10^8 stars in the Galactic bulge (Szymański et al. 2011), as well as fields in the disk and toward the Magellanic Clouds. The current phase of the OGLE project, OGLE-IV, is covering a significantly larger area and detecting many more events than OGLE-III. In the near future the Large Synoptic Survey Telescope (LSST; for a more detailed discussion see the LSST Science Book; LSST Science Collaboration 2009) will also detect large numbers of microlensing events.

There are currently no wide-area surveys for astrometric microlensing events and none planned in the foreseeable future. However, if an astrometric microlensing event could be predicted then a specific observing campaign could monitor the particular area of sky in which the event will occur. It is possible to determine astrometric parameters independently for NSs that can be observed as radio pulsars. For such pulsars it is therefore possible to predict times of microlensing events.

A further advantage is that the distance to the pulsar can be independently estimated. The properties of such a microlensing event would therefore be well constrained and would provide a direct measurement of the mass of the pulsar lens. Currently only a relatively small number of radio pulsars is known. However, future radio telescopes, such as the Five-hundred-meter Aperture Spherical Telescope (Nan et al. 2006) and the Square Kilometre Array (Johnston et al. 2007), will discover a significant fraction of all the potentially observable radio pulsars in our galaxy and will be able to determine the astrometric parameters precisely for many of these pulsars.

In the first part of this paper we study photometric NS lensing events. We calculate the expected event rates and the characteristic timescale of NS events and determine the fraction of total events caused by NSs. Previous studies (e.g., Wood & Mao 2005, hereafter WM05; Sartore & Treves 2010; Oslowski et al. 2008) were not based on the most up to date spatial and velocity distributions for the NS population (e.g., Hobbs et al. 2005; Faucher-Giguère & Kaspi 2006; Lorimer et al. 2006). NS lensing events are only a small fraction of the total number of events detectable in a lensing survey. We show that knowledge of the expected characteristic timescale of NS events can significantly improve identification of such events.

In the second part of the paper we make predictions for astrometric microlensing events caused by NSs. We provide expected event rates and determine the likely precision that could be achieved for NS masses. This has not been previously investigated (previous studies concentrated on stellar lenses, e.g., BE02). We conclude by discussing the implications of our results and providing predictions for future surveys.

2. PROPERTIES OF PHOTOMETRIC MICROLENSING CAUSED BY NSs

In this section, we investigate photometric microlensing events caused by NSs. NSs can lens emission from Galactic stellar objects and also from background galaxies. As Tian & Mao (2012) have already studied NS lensing faint background galaxies, we concentrate on Galactic background stellar objects. Our work follows the procedure described in WM05. In Section 2.1, we describe the spatial and velocity distribution of the NS population and the stellar models used in our simulations. We then present the event rates, the timescale distributions of microlensing events caused by NSs, and their fractional contribution to the Galactic event rates.

2.1. NS and Stellar Population Distributions

2.1.1. The Distribution of the NS Population

We assume that the NS number density is proportional to that of radio pulsars. In cylindrical coordinates originating at the Galactic Center (GC), the NS number density is expressed as

$$\rho(R, z) = A\left(\frac{R + R_1}{R_\odot + R_1}\right)^a \exp\left[-b\left(\frac{R - R_\odot}{R_\odot + R_1}\right)\right] \times \exp\left(-\frac{|z|}{E}\right), \quad (1)$$

where $R_1 = 0.55$ kpc, $a = 1.64$, $b = 4.01$, $E = 330$ pc, and the distance from the Sun to the GC is set to be $R_\odot = 8.0$ kpc. This assumes the radial distribution of NSs suggested by Yusifov & Küçük (2004). Such a radial distribution was also used in Faucher-Giguère & Kaspi (2006), and allows us to use their prediction for the number of potentially observable pulsars (i.e., NSs that are radio-loud and beamed toward us). For the z distribution we use the scale height obtained by Lorimer et al. (2006).

The total number of NSs in the Galaxy is still unclear. Following recent estimations (Keane & Kramer 2008), we normalize the parameter A to give a total NS number of 10^9. For potentially observable pulsars, A is normalized to give a total number of observable pulsars of 120,000 (Faucher-Giguère & Kaspi 2006). We note that this number does not account for the population of rotating radio transients (McLaughlin et al. 2006). Their inclusion would significantly increase the number of observable NSs (Keane & Kramer 2008).

We adopt a Gaussian model with $\sigma = 290\,\mathrm{km\,s^{-1}}$ (Faucher-Giguère & Kaspi 2006) for the distribution of the components of the NS velocities. As will be defined in Section 2.2, the timescale and event rate are inversely proportional and proportional to the lens–source relative transverse velocity, respectively, and therefore increasing or decreasing the σ of the NS velocity distribution will simply rescale the timescale and event rate. Although an exponential model is preferred in Faucher-Giguère & Kaspi (2006), the Gaussian model has also been shown to match well the velocity distribution of radio pulsars (Hobbs et al. 2005) and provides a straightforward distribution for us to use in our calculations. In the analysis below we use the Gaussian model by default, but for comparision we also give some results based on the exponential model.

2.1.2. Stellar Models

In order to determine the properties of the background stars we consider stellar populations in the bulge and in the disk. For the bulge distribution of stellar objects, we use the E2 model in Rattenbury et al. (2007). We truncate the bulge at a corotation radius $R_C = 3.5$ kpc (Bissantz & Gerhard 2002). The model is normalized to the observed value of the optical depth toward the Central Galactic Region (Popowski et al. 2005; Calchi Novati et al. 2008). The disk distribution of stellar objects is relatively well constrained, and we use the local vertical density model of Zheng et al. (2001), as extended to the whole Galactic disk by Han & Gould (2003).

We also need models of the lensing objects (both NSs and other objects). For the lens mass function, we follow a procedure identical to that described in WM05. This is based on a two part power-law distribution

$$\frac{dN}{dM} = k\left(\frac{M}{M_{\rm brk}}\right)^\alpha, \quad (2)$$

where $M_{\rm brk} = 0.7\,M_\odot$, $\alpha = -2.0$ for $M > M_{\rm brk}$, and $\alpha = -1.3$ for $M \leqslant M_{\rm brk}$.

We adopt the kinematic model of WM05, which describes the velocities of the lenses, sources, and the observer. The lens–source relative transverse velocity, v, is calculated according to Equations (7) and (8) in WM05. The conversion of velocities from Galactocentric cylindrical coordinates into solar-centric spherical coordinates is given by Equation (15) in Wang & Smith (2011).

2.2. The Photometric Microlensing Model

The timescale of a microlensing event is the time taken for a source to cross the Einstein radius of the lens, $r_{\rm E}$, and is defined as (Paczynski 1996)

$$t_{\rm E} = \frac{r_{\rm E}}{v}, \quad r_{\rm E} = \sqrt{\frac{4GM}{c^2}\frac{D_{\rm d}(D_{\rm s}-D_{\rm d})}{D_{\rm s}}}, \tag{3}$$

where G is the gravitational constant, c is the speed of light, $D_{\rm s}$ is the source distance, and $D_{\rm d}$ is the lens distance.

The event rate, Γ, is defined as the number of photometric microlensing events per unit time for a given number of background sources. The event rate depends on the background source number density, $\rho_{\rm s}(D_{\rm s})$, and the mass density of lensing objects, $\rho_{\rm m}(D_{\rm d})$. Following Kiraga & Paczynski (1994) and WM05, we assume that the fraction of stars brighter than some luminosity L is proportional to L^{β}, and then the event rate is expressed as

$$\Gamma = \frac{4G^{1/2}}{c}\int_0^{\infty} dD_{\rm s} D_{\rm s}^{2+2\beta}\rho_{\rm s}(D_{\rm s}) \frac{\int_0^{D_{\rm s}} dD_{\rm d}\rho_{\rm m}(D_{\rm d})v\left[D_{\rm d}(D_{\rm s}-D_{\rm d})/MD_{\rm s}\right]^{1/2}}{\int_0^{\infty} dD_{\rm s} D_{\rm s}^{2+2\beta}\rho_{\rm s}(D_{\rm s})}, \tag{4}$$

where v is the lens–source relative transverse velocity.

We use β to model numerous phenomena that are not explicitly included in the equation. To account for the luminosity function of the background sources, the optical survey sensitivity, and the Galactic extinction, we set $-3 \leqslant \beta \leqslant -1$ (Kiraga & Paczynski 1994). We also calculate our results with $\beta = 0$, which corresponds to the maximum possible event rate. This is a simplified approach, but has been applied by previous studies on the Galactic microlensing event rate and is valid as we only report basic properties of NS lensing events and do not attempt to predict the exact number of events detected with a particular set of survey parameters. Although extinction will clearly affect our estimates for the event rates, implementing this in a consistent manner is a very complex task (see, for example, Kerins et al. 2009). However, since extinction results in a change in the slope of the luminosity function, this can be reflected in the choice of the β parameter, i.e., large negative values of β can be used to account for high extinction. We consider stellar objects in the Galactic disk and in the bulge to be background sources. As the disk stars can have small distances, setting $-3 \leqslant \beta \leqslant -1$ will result in unreasonably small event rates. We account for this by always setting $\beta = 0$ for disk sources within 4.5 kpc from the observer.

To calculate the event rates and mean timescales, we use the adaptive Monte Carlo integration algorithms incorporated in the GNU Scientific Library.[6] In order to improve the calculation precision we use a sampling number of 10^7 over the multi-dimensional volume when we carry out the Monte Carlo integrations.

[6] http://gnu.org/software/gsl/

Table 1
The Event Rates Caused by Potentially Observable Radio Pulsars, in Units of $10^{-11}\,{\rm yr}^{-1}$

β	All-sky	$\lvert b\rvert < 5°$	$\lvert b\rvert > 5°$	GC	BW
0	5.0	5.7	1.3	8.0	4.4
−1	1.5	2.0	0.5	5.5	2.8
−2	0.9	1.2	0.4	2.0	1.4
−3	0.9	1.2	0.4	1.9	1.3

Note. To obtain the event rate for NS lenses, the numbers in this table should be multiplied by a factor of $10^9/\left(1.2\times10^5\right)$.

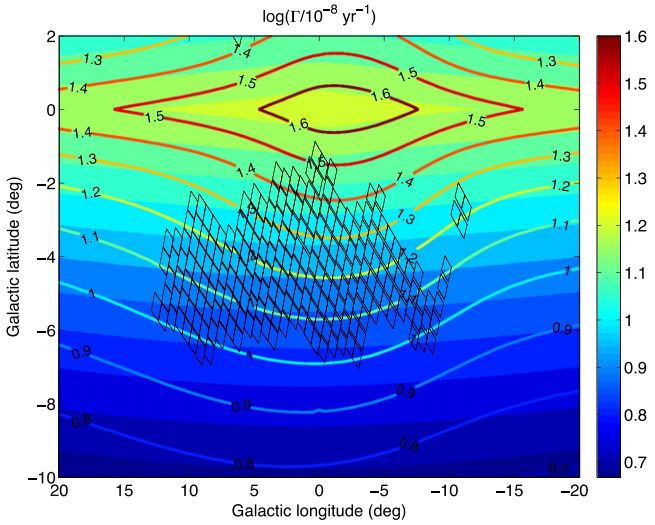

Figure 1. Map of the microlensing event rates caused by NSs, toward the central Galactic region. Contours with solid lines represent results for $\beta = -1$. Contours filled with colors represent results for $\beta = -2$. OGLE-III fields are shown with diamond symbols. Contour levels represent the event rate in logarithmic scaling, $\log(\Gamma/10^{-8}\,{\rm yr}^{-1})$.

2.3. Photometric Microlensing Results

2.3.1. Event Rates

Our results give a maximum possible all-sky averaged event rate ($\beta = 0$) of $4.2\times10^{-7}\,{\rm yr}^{-1}$ for NS lenses. Toward the GC and the Baade's window (BW)[7] region, this maximum event rate is $6.7\times10^{-7}\,{\rm yr}^{-1}$ and $3.6\times10^{-7}\,{\rm yr}^{-1}$, respectively. Setting $\beta = -1, -2, -3$, the all-sky averaged event rate is $1.3\times10^{-7}\,{\rm yr}^{-1}$, $7.5\times10^{-8}\,{\rm yr}^{-1}$, and $7.4\times10^{-8}\,{\rm yr}^{-1}$, respectively. In Table 1 we present the all-sky averaged event rate, rates for $|b| < 5°$ and $|b| > 5°$, and rates toward the GC and BW, for $\beta = 0, -1, -2, -3$ for 120,000 potentially observable radio pulsars. Since we have assumed that the population model for radio pulsars is identical to that of NSs, except for the normalization, this means that the event rates for potentially observable radio pulsars is a factor of $10^9/\left(1.2\times10^5\right)$ smaller than that of NSs. Using the exponential model proposed by Faucher-Giguère & Kaspi (2006), we obtained an all-sky averaged event rate for potentially observable radio pulsars of $4.2\times10^{-11}\,{\rm yr}^{-1}$ ($\beta = 0$), compared with $5.0\times10^{-11}\,{\rm yr}^{-1}$ for the Gaussian model.

[7] $(l, b) = (1.16°, -2.75°)$; l and b are the Galactic longitude and latitude.

We show in Figure 1 the expected NS event rates in the central Galactic region. The contour levels represent the event rate using logarithmic scaling, log ($\Gamma/10^{-8}$ yr^{-1}). Two sets of contours are shown. Contours for $\beta = -1$ are shown with solid lines. Contours for $\beta = -2$ are shown as shaded regions. As expected, the event rate is higher on the Galactic plane and decreases at higher Galactic latitudes. As β varies from −1 to −2, the distribution of the event rates becomes flatter, and the rate decreases much more significantly on the Galactic plane compared to that at a higher Galactic latitude region.

The reduction in event rates as β decreases and the flattening of the event rate distribution can be explained as follows.

1. Decreasing β implies that fewer distant sources contribute to the event rate. Therefore the total event rate will decrease as β decreases.
2. Toward the GC the stellar density is higher than in the Galactic disk. Decreasing β therefore has a larger effect in the GC region than elsewhere.
3. Sources in the bulge have a high velocity dispersion. Therefore decreasing β effectively removes more high-velocity stellar objects in the bulge compared with the disk.
4. Sources on the far side of the Galactic disk rotate in the direction opposite the observer. These sources therefore contribute a significant number of events as their relative velocities to the NS lenses are high. Decreasing β removes these distant background sources.

OGLE-III fields[8] are shown in Figure 1 with diamond symbols. For 340 × 10^6 background sources (Szymański et al. 2011) and taking $\beta = -1$, we predict there should have been around 50 NS events per year and there is about a 6% chance that there has been an event from a potentially observable radio pulsar during the 9 yr duration of the survey. The current phase of the OGLE project (OGLE-IV) started in 2010 and is now detecting around four times as many microlensing events per year in the bulge compared to OGLE-III.[9] This could therefore detect around two hundred NS events per year and, given the event rate for potentially observable radio pulsars, there is a ∼23% chance it will detect one by the end of the decade. For future deeper and wider optical surveys, the prospects of discovering pulsar microlensing events are promising. For example, LSST is expected to monitor $\sim 10^{10}$ background Milky Way sources (Ivezić et al. 2012). Taking $\beta = -1$, we predict there will be ∼1000 events caused by NSs per year and ∼1.5 events caused by potentially observable pulsars per decade.

Note that our photometric event rates are likely to underestimate the actual number of observable events. This is because our calculations are based on the definition of a microlensing event as one in which the lens passes within one Einstein radius of the source, corresponding to an amplification of 0.32 mag. However, in practice it is possible to detect events with much weaker amplification. If we instead define an event as one in which the amplification is 0.1 mag, then the event rate will be ∼70% higher. There is also the fact that the actual number of source stars may be underestimated due to blending from unresolved source stars (e.g., Smith et al. 2007).

[8] Data from http://ogle.astrouw.edu.pl/.
[9] http://ogle.astrouw.edu.pl/ogle4/ews/ews.html

2.3.2. Timescale Distributions

By restricting the Monte Carlo integrations in a parameter space corresponding to a certain timescale, we can directly obtain the event rate caused by NSs as a function of the timescale. This is shown in Figure 2 for $\beta = 0$. The timescale distributions for the all-sky averaged event rate are shown as the solid line. The event rates toward the GC and BW are presented as dotted and dashed lines, respectively. We note that the distributions have asymptotic power-law tails following the expected form given by Mao & Paczynski (1996). In all cases the event rate peaks at a timescale of ∼12 days. The mean timescales for the all-sky averaged, GC, and BW event rates are ∼19.7, 19.3, and 19.4 days, respectively. For comparison we also overlay the prediction from WM05 toward the BW, which has a mean timescale of 47.3 days. Our new results therefore imply that the majority of NS events will have shorter timescales than predicted by WM05, which is mainly because of the relatively high velocity of NSs. Using the exponential model, we obtained a mean timescale for the all-sky averaged event rate of ∼23.7 days.

In Figure 3, we show the effects of changing β on events toward the GC. The difference in the event rate between $\beta = -1$ and −2 is much larger than for other β values because the background source density starts to decrease with increasing distance according to the $D_s^{2+2\beta}$ term in Equation (4). Below the mean timescale the choice of β has little effect on the results. β does affect the longer timescales with, as expected, smaller event rates as β decreases. However, the mean timescale is slightly dependent on β, with the mean timescales being 19.3, 17.9, 13.5, and 13.2 days for $\beta = 0$ to −3, respectively. This shift was not initially expected, as decreasing β reduces the averaged transverse velocity between the sources and lenses, leading to an expected decrease in the number of short-duration events. In order to understand this result, we calculated the Einstein radii averaged over all lenses and the averaged transverse velocity between the lenses and sources. We found that as β decreased, the averaged Einstein radii decreased faster than the reduction in the averaged transverse velocity. This implies that the resulting lensing events will occur with lenses that have smaller Einstein radii and therefore the timescale of these events will be shorter.

WM05 predicted the averaged timescales of all (not just NS) Galactic events as a function of Galactic coordinates. The short-duration events we are predicting for NS lenses will lower the mean timescale of these events. Our map is presented in Figure 4 and can be compared with Figure 3 in WM05. The solid contours represent $\beta = -1$ and the shaded regions $\beta = -2$. The OGLE-III fields are shown with diamond symbols. Our averaged timescales toward the BW are 23.3, 23.9, and 36.5 days for $\beta = 0, -1, -2$, respectively. For $\beta = 0, -1$, our results are similar to, but slightly smaller than, the corresponding results in WM05 and generally agree with the actual measurement of 28.1 ± 4.3 days (Sumi et al. 2006) from the OGLE survey.

2.3.3. Fractional Contribution to the Galactic Event Rate

We have shown that NS events have relatively short timescales. Sumi et al. (2011) showed that Jupiter-mass objects have even shorter timescales, while other stellar objects can have longer timescales. In this subsection, we consider the

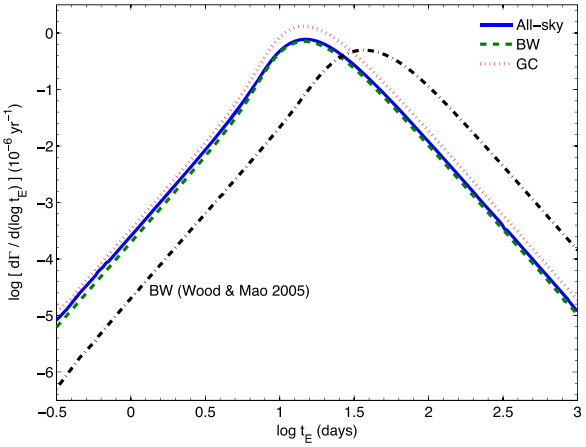

Figure 2. Microlensing event rates caused by NSs as a function of timescale. The solid, dotted, and dashed lines represent the all-sky averaged event rate and the event rates toward the GC and BW, respectively. In comparison, the timescale distribution for NSs toward the BW based on WM05's model is shown as indicated.

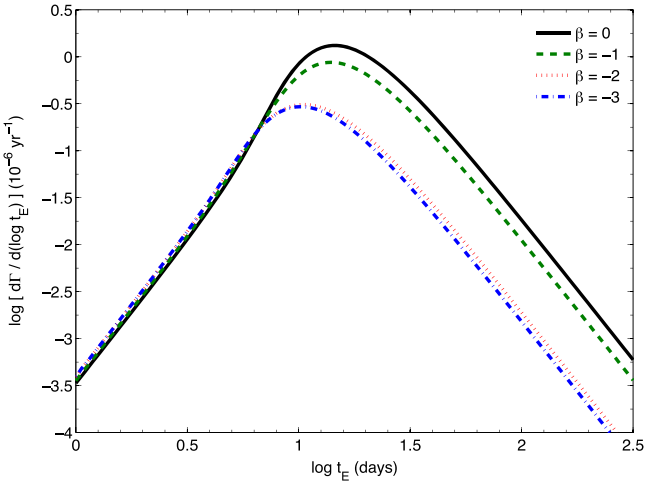

Figure 3. Microlensing event rates caused by NSs as a function of timescale toward the GC. The solid, dashed, dotted, and dotted–dashed lines represent event rates for $\beta = 0, -1, -2, -3$, respectively.

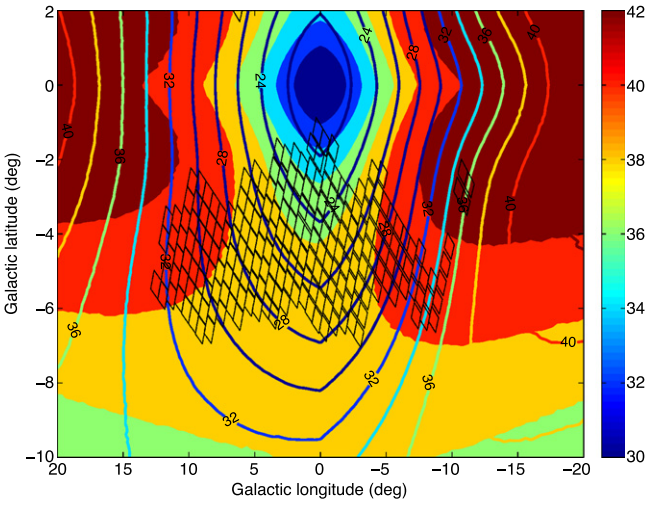

Figure 4. Maps of the averaged timescales of Galactic microlensing events. Contours with solid lines represent results for $\beta = -1$. Contours filled with colors represent results for $\beta = -2$. Contour levels represent averaged timescales in unit of days. OGLE-III fields are shown with diamond symbols.

fraction of Galactic events that are caused by NS lenses for different timescales.

In Figure 5 we present the fraction of events that are caused by NSs as a function of timescale. The solid line refers to events toward the BW and the dashed line toward the GC. We also show results for two off-GC directions, $(l, b) = (-20^\circ, 0^\circ)$ and $(l, b) = (0^\circ, -10^\circ)$. For $(l, b) = (-20^\circ, 0^\circ)$ (on the disk, but away from the bulge), NS lenses contribute up to ∼40% of the events that last less than ∼10 days, but we note that the total number of events in this direction is low. For the three other sky positions, the fractional contribution exhibits a clear peak around a timescale of ∼15 days and decreases at higher and lower timescales. Our results do not agree with earlier predictions from WM05 (shown as a dotted–dashed line in the figure). Their work led to very small fractional contributions from NSs at ∼15 days and much larger fractional contributions on timescales of months to years. On the contrary, in our calculations we have found that NSs mainly contribute to short-duration Galactic events because of their relatively high velocities (a factor not considered by WM05). Away from the Galactic bulge region, as the rate of short-duration Galactic events drops, the fractional contribution from NSs increases rapidly at short timescales.

In Figure 6 we show the fractional contribution toward the GC from NSs for different values of β. In all cases the fractional contribution peaks at ∼10 days and we cannot reproduce the WM05 results by modifying β. As β decreases the fractional contribution on timescales of ∼10 days increases. For $\beta = -3$ almost all events at this timescale would be caused by NS lenses.

The fractional contribution from NS lenses changes as a function of sky position. Figure 7 shows the fractional contributions from NSs in the central Galactic region. Contours indicated with solid lines are for $\beta = -1$. Contours shown as shaded regions are for $\beta = -2$. The OGLE-III fields are indicated using diamond symbols. The fractional contribution from NSs clearly varies with Galactic latitude, with higher contributions from NSs occurring away from the Galactic bulge.

Averaged over all timescales and over the entire sky we find that NSs contribute ∼5.4% ($\beta = 0$) of the total number of Galactic events. In Table 2, we present the fractional contribution to the total averaged event rate from different types of lensing objects. The different objects considered are brown dwarfs (BDs), main-sequence stars (MSs), white dwarfs (WDs), and black holes (BHs). We also show contributions for different values of β. For $\beta = 0$, the NS contribution overall is small, however for other values of β the contribution from NSs is much more significant. By increasing and decreasing the σ of the NS velocity distribution by 30%, we got a fractional contribution from NSs of approximately 6.5% and 3.7%, respectively ($\beta = 0$). Using the exponential model, the fractional contribution from NSs is approximately 4.2% ($\beta = 0$).

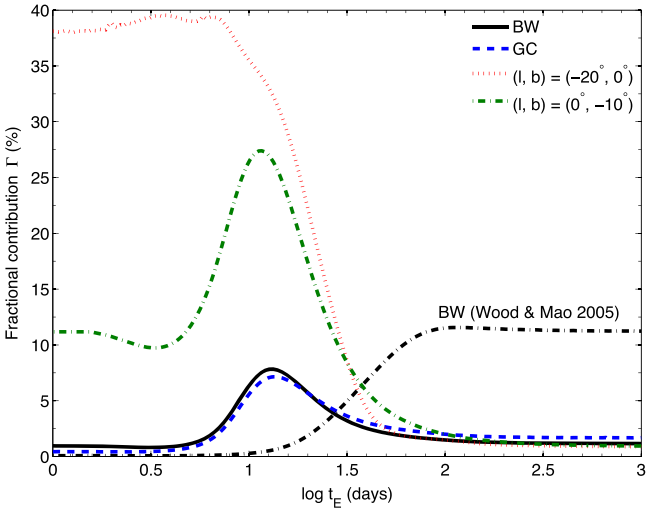

Figure 5. Fractional contributions to the total Galactic event rate, as a function of the event timescale, from NSs. The solid, dashed, dotted, and dotted–dashed lines show the contribution from NSs toward the BW, GC, and off-GC directions $(l, b) = (-20°, 0°)$ and $(l, b) = (0°, -10°)$, respectively. In comparison, the fractional contribution from NSs toward the BW based on WM05's model is shown as indicated.

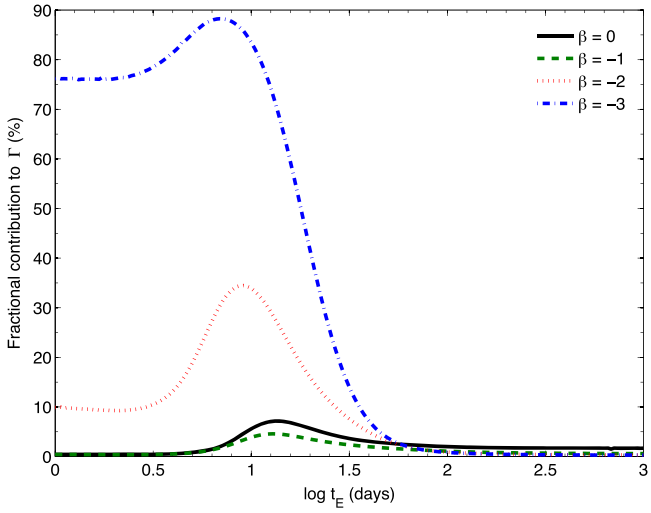

Figure 6. Fractional contributions to the total Galactic event rate, as a function of the event timescale, from NSs, toward the GC. The solid, dashed, dotted and dashed-dotted lines represent the contributions for $\beta = 0, -1, -2, -3$, respectively.

3. MASS MEASUREMENT THROUGH ASTROMETRIC MICROLENSING

We have investigated the properties of photometric microlensing events caused by NSs. However, the photometric microlensing event rate caused by potentially observable radio pulsars is only ∼2 per decade for 10^{10} background sources. As astrometric microlensing has a larger cross-section than photometric microlensing, more astrometric microlensing events are expected to be detected. It is not currently feasible to carry out large-scale astrometric microlensing surveys. A more promising way to search for events caused by observable radio pulsars is to use the known pulsar astrometric parameters to make an initial guess for when and where microlensing events will occur. This approach can also be applied to photometric microlensing, but the larger cross-section means that it is especially promising for astrometric detections.

The method we used to estimate the photometric microlensing event rate is also valid for astrometric lensing, but the larger cross-section must be accounted for. The cross-section and the amplitude of an astrometric microlensing event can be characterized by the impact parameter, u_0, which is defined as the smallest angular separation between the lens and the source in units of the angular Einstein radius. The astrometric microlensing event rate will simply be our determination of the photometric event rate scaled by the increase in the cross-section. For instance, if the cross-section is ∼10 times larger ($u_0 = 10$, discussed in more detail in Section 3.2) then, for 120,000 potentially observable radio pulsars, the all-sky averaged event rate with $\beta = -1$ will then be ∼1.5 yr^{-1} for 10^{10} background sources.

3.1. Astrometric Microlensing Model

BE02 presented methods to determine the precision that could be achieved for stellar lens mass estimates obtained through astrometric microlensing. They showed that there was a total of 11 parameters to completely parameterize such

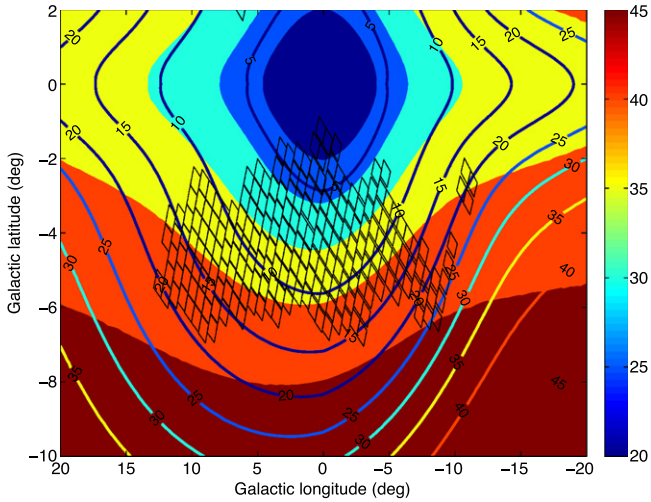

Figure 7. Maps of the percentage contribution to the total Galactic microlensing event rates from NSs. Contours with solid lines represent results for $\beta = -1$. Contours filled with colors represent results for $\beta = -2$. Contour levels represent the percentage contribution in percent. OGLE-III fields are shown with diamond symbols.

Table 2
Percentage Contributions to the Total Event Rate, from Different Types of Lenses

	Type of Lens				
β	BD	MS	WD	BH	NS
			(Percent)		
0	16.7	60.5	16.5	0.9	5.4
−1	15.8	57.2	15.5	0.9	10.6
−2	10.6	38.2	10.4	0.5	40.3
−3	10.0	36.0	9.8	0.5	43.7
0 (WM05)	17.2	62.1	16.9	0.9	2.9

Note. Results for $\beta = -1, -2, -3$ are also presented. For comparison, results based on WM05's model are also shown.

events. We apply their methods to determine the precision achievable for observable radio pulsars.

For radio pulsar lenses, the positions, proper motions, and distances of lenses can, in principle, be measured or estimated through radio observations. Pulsar positions and proper motions can be determined either through radio pulsar timing or interferometric observations. For millisecond pulsars that have been observed over many years, the precision of positions and proper motions determined through pulsar timing could reach $\leqslant$1 mas and $\leqslant$1 mas yr^{-1}, respectively (e.g., Verbiest et al. 2008). For pulsars whose positions and proper motions cannot be obtained precisely through pulsar timing, interferometric observations can be used.[10] In our model, we consider an ideal case in which we assume that the radio pulsar lens positions and proper motions are known parameters and we neglect their uncertainties. The implications of these assumptions are discussed at the end of Section 3.2.

Pulsar distances are much harder to measure than positions or proper motions. For some pulsars precise distances can be obtained from measurements of the parallax. For most pulsars distances can only be estimated from dispersion measures. The conversion from dispersion measure to distance depends on models of the distribution of free electrons in the Galaxy. As such models are not very well constrained, this results in distance uncertainties of around 20% (Taylor & Cordes 1993). Although models of the Galactic free electron density are continually being improved (e.g., Cordes & Lazio 2002), it is not clear whether distances will be measured sufficiently for most pulsars at the time that astrometric lensing events from pulsars are detected. Therefore, in our analysis we discuss two models. In the first model, which we label as Model $D_{\rm psr}^{\rm known}$, we assume that the pulsar distance is known. In the second model, Model $D_{\rm psr}^{\rm unknown}$, we assume that it is not.

For Model $D_{\rm psr}^{\rm known}$, six independent parameters need to be computed from the data. These are the position ($\boldsymbol{\theta}_{\rm s,0}$), proper motion ($\boldsymbol{\mu}_{\rm s}$), and parallax ($\pi_{\rm s}$) of the background source and the mass (M) of the lens. We note that it is possible that the astrometric parameters for the background source are also precisely known. If true, then the only unknown parameter will be the mass. For this work, we assume that these parameters do need to be determined from the data. For Model $D_{\rm psr}^{\rm unknown}$, we have an additional parameter, the pulsar parallax ($\pi_{\rm l}$).

As an example, we consider a specific pulsar, PSR B1929+10. This pulsar has a large proper motion (103 mas yr^{-1}; Chatterjee et al. 2004) and lies in close projection to a number of potential background source stars, with seven objects within 5 arcsec according to our catalog comparison between known radio pulsars[11] (Manchester et al. 2005) and source tables from the UKIRT Infrared Deep Sky Survey (UKIDSS; Lawrence et al. 2007). The distance to this pulsar is 0.36 kpc (Chatterjee et al. 2004). We assume that this pulsar is likely to pass one of the background sources and could be studied with an astrometric monitoring campaign that carries out observations of the background source with a uniform observing cadence over a period of 4 yr (centered on the time of closest angular separation between the lens and the source). Following BE02, we assume that the background source is at a distance of 5 kpc with a proper motion of 7 mas yr^{-1}.

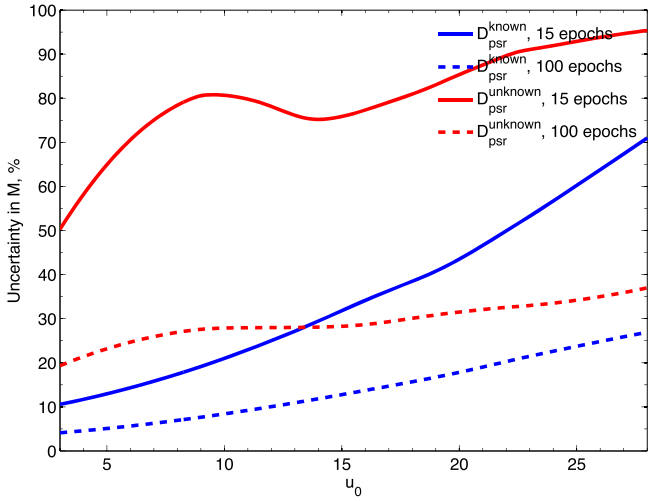

Figure 8. Percentage error in estimation of M as a function of impact parameter u_0. We set $M = 1.4\ M_\odot$ and $\sigma = 150\ \mu$as. The solid and dashed lines represent the errors with 15 and 100 observation epochs, respectively. The blue and red lines represent models for which pulsar distances can be measured precisely from external methods (Model $D_{\rm psr}^{\rm known}$, blue) and for which pulsar distances need to be computed from the microlensing data (Model $D_{\rm psr}^{\rm unknown}$, red).

We note that our selection of lens and source proper motions and distances will not limit the generality of our analysis, since the amplitude of an astrometric microlensing event is only characterized by u_0. However, the uncertainty on the mass measurements will depend on various parameters that need to be assumed in our modeling. The first is the pulsar mass. In our analysis, we use $M = 1.4\ M_\odot$ as a typical pulsar mass, but also trial different values. We also require an estimate of the astrometric accuracy that can be achieved for the background stellar object. We trial two possible values, $\sigma = 150$ and 450 μas. $\sigma = 150\mu$as corresponds to a relatively bright star at around $V = 16$ mag for the *Gaia* satellite.[12] Future telescopes such as the *Wide-Field Infrared Survey Telescope* (*WFIRST*) have the potential to obtain astrometric precision of a few tenths of a mas for even fainter stars (e.g., Spergel et al. 2013). Finally, the uncertainty also depends on the number of epochs that are observed during the four year monitoring program. In the results below we trial a range of possible values.

3.2. Mass Determination Results

Figure 8 shows the uncertainties in M as a function of the dimensionless impact parameter u_0 for the two models (in which the pulsar distance is known or not). We present results for our two models with different samplings (for 15 and 100

[10] We note that the dynamical solar system ephemeris used for pulsar timing is different from the International Celestial Reference Frame (ICRF). Madison et al. (2013) computed a transformation between the ICRF and pulsar timing frames and quantitatively discussed how the transformation will improve in the coming years.

[11] http://atnf.csiro.au/research/pulsar/psrcat

[12] The end-of-mission parallax error for such a star is around 20–40 μas. The single epoch positional precision is significantly worse. We estimate how much worse using information provided on http://cosmos.esa.int/web/gaia/science-performance as follows. The positional precision for a single epoch measurement is more precise than the parallax precision by a factor of 0.743, but the single epoch precision is a factor of 4.3 times worse than that available at the end of the mission. From this we estimate that the single epoch positional precision is around three times worse. We also need to incorporate a factor of $\sqrt{2}$ to account for the fact at each epoch *Gaia* only measures the one-dimensional position along the scanning direction. This gives an effective two-dimensional astrometric precision of around 90–180 μas. Note that for faint stars ($V = 20$ mag) the end-of-mission parallax precision drops to around 130–600 μas, meaning that the effective two-dimensional astrometric accuracy will be around 0.5–3 mas.

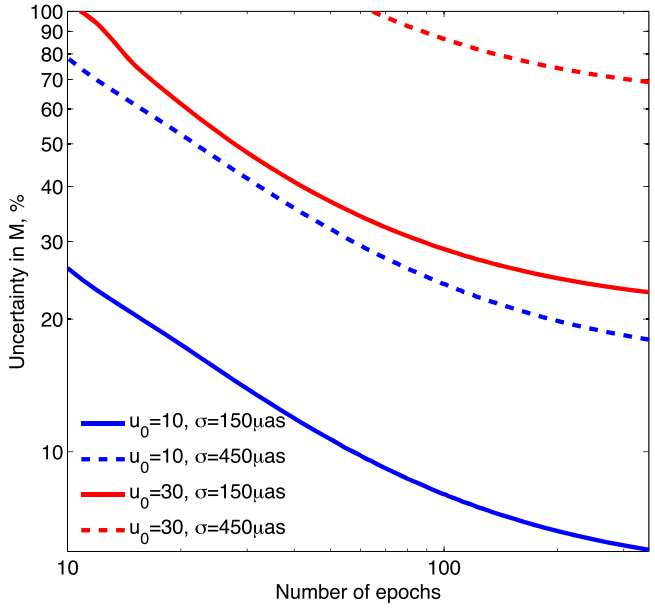

Figure 9. Percentage error in estimation of M as a function of the number of observation epochs, for Model $D_{\rm psr}^{\rm known}$. Results for different u_0 and σ are shown.

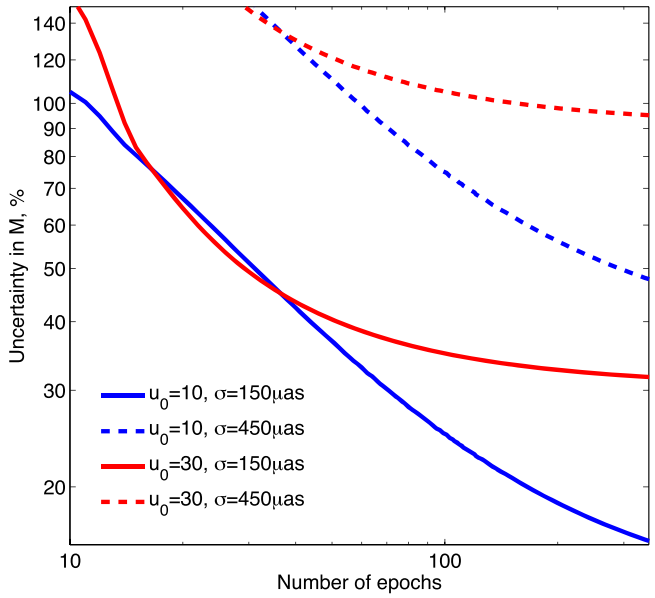

Figure 10. Percentage error in estimation of M as a function of the number of observation epochs, for Model $D_{\rm psr}^{\rm unknown}$. Results for different u_0 and σ are shown.

observation epochs). There is a large variation in the ability to determine the pulsar mass. The uncertainties in M increase with increasing u_0 and decrease with the number of epochs. If the pulsar distance is known then its mass could be determined at least two times better than if the mass is not known. Note that for *Gaia* the average number of epochs is around 70 (de Bruijne 2012).

Figures 9 and 10 show the uncertainties in M as a function of the number of observation epochs. In Figure 9 we assume that the pulsar distance is known, while in Figure 10 we assume it is unknown. For both figures, we present results for $u_0 = 10$ and $u_0 = 30$, and for $\sigma = 150\,\mu$as and $\sigma = 450\,\mu$as. For more than ~100 epochs the uncertainty is approximately constant. More frequent sampling is therefore not necessary and will not improve the mass determination. As the astrometric precision improves from $450\,\mu$as to $150\,\mu$as, the uncertainty in M decreases by more than a factor of 2. Clearly, it is therefore essential that the background source is monitored with high-precision astrometry.

In Figure 11, we set different pulsar masses and show the uncertainties in M as a function of the number of epochs for Model $D_{\rm psr}^{\rm known}$. In addition to a typical pulsar mass of $1.4\,M_\odot$, we also show results for an extremely low-mass case, $0.4\,M_\odot$, and a relatively high-mass case, $2.4\,M_\odot$. We set $u_0 = 10$ and $\sigma = 450\,\mu$as. As the pulsar mass increases the uncertainties become smaller. For the high-mass case, $M = 2.4\ M_\odot$, the uncertainty is six times smaller than that of the low-mass case, $M = 0.4\,M_\odot$.

In the analysis above, we have presented results for an ideal case in which we treat pulsar positions and proper motions as precisely determined values and we neglect their errors. If the pulsar astrometric parameters are poorly known then those parameters would need to be included in the model when determining the lensing event properties. This would significantly degrade the mass determination precision. Here, we investigate an intermediate case in which the astrometric parameters have been measured, but do have small uncertainties. We therefore model them as additional astrometric uncertainties of background sources and then apply the same method described above to estimate the uncertainty in pulsar masses. We assume that the uncertainties on the pulsar position and proper motion measurements are 0.01 mas and 0.1 mas yr^{-1}, respectively. This is similar to that obtainable with current very long baseline interferometry (VLBI) results (e.g., Deller et al. 2009). For Model $D_{\rm psr}^{\rm known}$, assuming $u_0 = 10$ and 50 epochs, the uncertainty on the mass measurement increases slightly from 10% to 12% compared with our earlier analysis. For larger pulsar position and proper motion errors of 0.1 mas and 1 mas yr^{-1}, the uncertainty of the mass measurement increases to 22%. Therefore, we conclude that the errors of pulsar position and proper motion can introduce additional uncertainties to pulsar mass measurements, but the effect is relatively small and can be significantly reduced by precise pulsar position and proper motion measurements already achievable with current VLBI observations.

4. CONCLUSIONS

A number of current and future surveys are carrying out photometric monitoring campaigns of the Galactic bulge and disk, such as OGLE-IV, Vista Variable in the Via Lactea (Minniti et al. 2010), and *WFIRST* (Spergel et al. 2013). In the near future the LSST (Ivezic et al. 2008) will monitor ~10,000 square degrees of sky using pairs of 15 s exposures twice per night every three nights on average. This will lead to a typical 5σ depth for point sources of $r \sim 24.5$ (AB). Currently it is unclear to what extent LSST will survey the Galactic disk and bulge. Even without large portions of the bulge and disk, LSST will monitor 10 billion Milky Way stars and if a strategy is chosen to include the disk and bulge, then this number will increase significantly. A specific 3 yr *HST* program (192 orbits) to detect microlensing events caused by non-luminous isolated black holes and NSs in the direction of the Galactic bulge has also been proposed (Sahu et al. 2012).

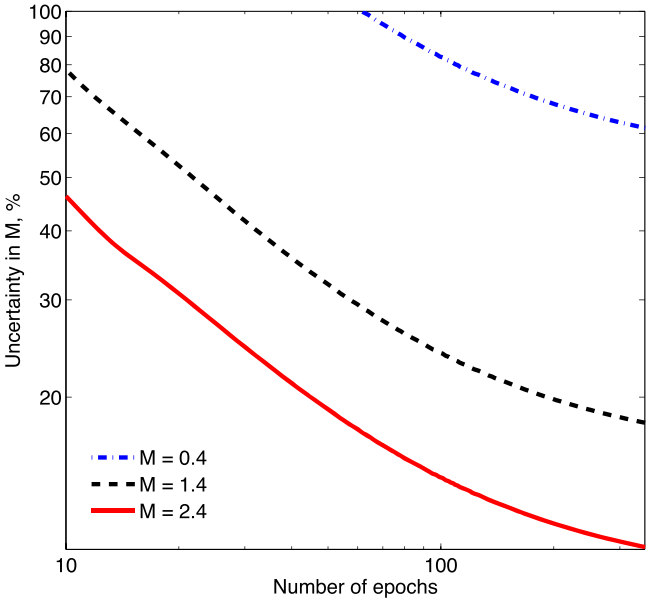

Figure 11. Percentage error in estimation of M as a function of the number of observation epochs, for Model $D_{\rm psr}^{\rm known}$. Results for pulsar masses of 0.4, 1.4, and 2.4 $M_{\odot}$ are shown.

Our modeling has shown the following.

1. The timescale of microlensing events caused by NSs is much shorter (∼20 days) than previously thought.
2. Events near the Galactic center that have a timescale of ∼15 days will contribute to approximately 7% of the total number of events. Away from the bulge region the fractional contribution for events with timescales of <20 days will increase to around 40%.
3. For an astrometric microlensing event caused by a known radio pulsar, pulsar masses could be determined with a precision of ∼10% if pulsar distances are known. With a sufficient number of observations of the event, the mass could be measured to ∼25% if the distance is not known.

For ongoing and upcoming surveys, we recommend the following.

1. To maximize NS events in the microlensing data set, surveys of the Galactic disk and bulge should be carried out.
2. NS events should be identified by searching for short-duration (∼20 days) events (instead of long duration events that had been previously considered) and radio telescopes should observe the possible candidates in order to identify radio pulsars.
3. As new pulsars are discovered, their astrometric parameters should be determined precisely and compared with catalogs of stellar positions. If a lensing event is likely then an astrometric lensing monitoring campaign should be carried out around the predicted time of the event.
4. Although these targeted campaigns are clearly the best approach to detect astrometric microlensing events from potentially observable radio pulsars, the prospects for ESA's *Gaia* mission (de Bruijne 2012) are not negligible. In total *Gaia* will observe ∼10^9 stars and so, according to our estimates, this equates to around one such event over the lifetime of the mission (5 yr).

In the more distant future, large radio telescopes will have discovered most of the potentially observable radio pulsars in the Milky Way. It is therefore likely that the mass of isolated NSs will be measurable through microlensing events, leading to improved knowledge of the pulsar population. Extremely high-mass and low-mass pulsars can then be studied in detail to provide new insight into the NS interior.

We acknowledge useful discussions with Dr. Jian Wang and members of pulsar group at PKU. S.D. is supported by the China Scholarship Council (CSC). M.C.S. acknowledges financial support from the CAS One Hundred Talent Fund and NSFC grants 11173002 and 11333003. This work is partially supported by the Gaia Research for European Astronomy Training (GREAT-ITN) Marie Curie network, funded through the European Union Seventh Framework Programme (FP7/2007-2013) under grant agreement No. 264895. G.H. is a recipient of a Future Fellowship from the Australian Research Council. This work is also supported by the National Natural Science Foundation of China (11225314), the National Basic Research Program of China (2012CB821801), the Strategic Priority Research Program "The Emergence of Cosmological Structures" of the Chinese Academy of Sciences, grant No. XDB09000000. This research has made use of NASA's Astrophysics Data System.

REFERENCES

Antoniadis, J., Freire, P. C. C., Wex, N., et al. 2013, Sci, 340, 448
Belokurov, V. A., & Evans, N. W. 2002, MNRAS, 331, 649
Bissantz, N., & Gerhard, O. 2002, MNRAS, 330, 591
Calchi Novati, S., de Luca, F., Jetzer, P., Mancini, L., & Scarpetta, G. 2008, A&A, 480, 723
Chatterjee, S., Cordes, J. M., Vlemmings, W. H. T., et al. 2004, ApJ, 604, 339
Cordes, J. M., & Lazio, T. J. W. 2002, arXiv:astro-ph/0207156
Dai, S., Xu, R. X., & Esamdin, A. 2010, MNRAS, 405, 2754
de Bruijne, J. H. J. 2012, Ap&SS, 341, 31
Deller, A. T., Tingay, S. J., Bailes, M., & Reynolds, J. E. 2009, ApJ, 701, 1243
Demorest, P. B., Pennucci, T., Ransom, S. M., Roberts, M. S. E., & Hessels, J. W. T. 2010, Natur, 467, 1081
Faucher-Giguère, C.-A., & Kaspi, V. M. 2006, ApJ, 643, 332
Han, C., & Gould, A. 2003, ApJ, 592, 172
Hobbs, G., Lorimer, D. R., Lyne, A. G., & Kramer, M. 2005, MNRAS, 360, 974
Horvath, J. E. 1996, MNRAS, 278, L46
Ivezić, Ž, Beers, T. C., & Jurić, M. 2012, ARA&A, 50, 251
Ivezic, Z., Tyson, J. A., Abel, B., et al. 2008, arXiv:0805.2366
Johnston, S., Bailes, M., Bartel, N., et al. 2007, PASA, 24, 174
Keane, E. F., & Kramer, M. 2008, MNRAS, 391, 2009
Kerins, E., Robin, A. C., & Marshall, D. J. 2009, MNRAS, 396, 1202
Kiraga, M., & Paczynski, B. 1994, ApJL, 430, L101
Lai, X.-Y., & Xu, R.-X. 2011, RAA, 11, 687
Lawrence, A., Warren, S. J., Almaini, O., et al. 2007, MNRAS, 379, 1599
Lorimer, D. R., Faulkner, A. J., Lyne, A. G., et al. 2006, MNRAS, 372, 777
LSST Science Collaboration Abell, P. A., Allison, J., et al. 2009, arXiv:0912.0201
Madison, D. R., Chatterjee, S., & Cordes, J. M. 2013, ApJ, 777, 104
Manchester, R. N., Hobbs, G. B., Teoh, A., & Hobbs, M. 2005, AJ, 129, 1993
Mao, S., & Paczynski, B. 1996, ApJ, 473, 57
McLaughlin, M. A., Lyne, A. G., Lorimer, D. R., et al. 2006, Natur, 439, 817
Minniti, D., Lucas, P. W., Emerson, J. P., et al. 2010, NewA, 15, 433
Nan, R.-D., Wang, Q.-M., Zhu, L.-C., et al. 2006, ChJAS, 6, 304
Oslowski, S., Moderski, R., Bulik, T., & Belczynski, K. 2008, A&A, 478, 429
Özel, F., Psaltis, D., Ransom, S., Demorest, P., & Alford, M. 2010, ApJL, 724, L199
Paczynski, B. 1996, ARA&A, 34, 419
Popowski, P., Griest, K., Thomas, C. L., et al. 2005, ApJ, 631, 879

Rattenbury, N. J., Mao, S., Sumi, T., & Smith, M. C. 2007, MNRAS, 378, 1064
Sahu, K. C., Albrow, M., Anderson, J., et al. 2012, American Astronomical Society Meeting Abstracts 220 307.03
Sartore, N., & Treves, A. 2010, A&A, 523, A33
Schwarz, D. J., & Seidel, D. 2002, A&A, 388, 483
Smith, M. C., Woźniak, P., Mao, S., & Sumi, T. 2007, MNRAS, 380, 805
Spergel, D., Gehrels, N., Breckinridge, J., et al. 2013, arXiv:1305.5422
Sumi, T., Woźniak, P. R., Udalski, A., et al. 2006, ApJ, 636, 240
Sumi, T., Kamiya, K., Bennett, D. P., et al. 2011, Natur, 473, 349
Szymański, M. K., Udalski, A., Soszyński, I., et al. 2011, AcA, 61, 83
Taylor, J. H., & Cordes, J. M. 1993, ApJ, 411, 674
Tian, L., & Mao, S. 2012, MNRAS, 427, 2292
Udalski, A. 2003, AcA, 53, 291
Verbiest, J. P. W., Bailes, M., van Straten, W., et al. 2008, ApJ, 679, 675
Wang, J., & Smith, M. C. 2011, MNRAS, 410, 1135
Weber, F. 2005, PrPNP, 54, 193
Wood, A., & Mao, S. 2005, MNRAS, 362, 945
Xu, R. 2010, IJMPD, 19, 1437
Yusifov, I., & Küçük, I. 2004, A&A, 422, 545
Zheng, Z., Flynn, C., Gould, A., Bahcall, J. N., & Salim, S. 2001, ApJ, 555, 393